Journal of Neuroscience Methods 207 (2012) 189–199

Contents lists available at SciVerse ScienceDirect

Journal of Neuroscience Methods

journal homepage: www.elsevier.com/locate/jneumeth

Computational Neuroscience

Volume conduction effects in brain network inference from electroencephalographic recordings using phase lag index

Luis R. Peraza[a,*], Aziz U.R. Asghar[b,c], Gary Green[b], David M. Halliday[a,*]

[a] Intelligent Systems Group, Department of Electronics, University of York, YO10 5DD, UK
[b] York Neuroimaging Centre, University of York, YO10 5DG, UK
[c] Hull York Medical School, University of Hull, HU6 7RX, UK

ARTICLE INFO

Article history:
Received 11 July 2011
Received in revised form 1 April 2012
Accepted 6 April 2012

Keywords:
Brain networks
Phase lag index
Coherence
Electroencephalography
Volume conduction

ABSTRACT

In this paper, we test the performance of a synchronicity estimator widely applied in Neuroscience, phase lag index (PLI), for brain network inference in EEG. We implement the four sphere head model to simulate the volume conduction problem present in EEG recordings and measure the activity at the scalp of surrogate sources located at the brain level. Then, networks are estimated under the null hypothesis (independent sources) using PLI, coherence (R) and phase coherence (PC) for the volume conduction and no volume conduction (NVC) cases. It is known that R and PC are highly influenced by volume conduction, leading to the inference of clustered grid networks. PLI was designed to solve this problem. Our simulations show that PLI is partially invariant to volume conduction. The networks found by PLI show small-worldness, with a clustering coefficient higher than random networks. On the contrary, PLI-NVC obtains networks whose distribution is closer to random networks indicating that the high clustering shown by PLI networks are caused by volume conduction. The influence of volume conduction in PLI might lead to biased results in brain network inference from EEG if this behaviour is ignored.

1. Introduction

In recent years, the interest of the Neuroscience community in brain networks inference has increased. Small-world networks in particular have been found in the nervous systems of several simple and complex organisms, for instance *C. elegans* (Watts and Strogatz, 1998), the cat (Scannell et al., 1995), the monkey (Young, 1992), and the human (Sporns and Zwi, 2004; Sporns and Honey, 2006; He et al., 2007; Zhang and Zhang, 2009).

Brain network research is aided by imaging technologies such as functional magnetic resonance imaging (fMRI), magnetoencephalography (MEG) and electroencephalography (EEG). Much of the current work is focused on brain synchronization, searching for different brain regions in continuous interaction. This interaction can be causal, where a small delay can be detected between two sources, or fully synchronized where no delay is present. Brain network theory has evolved mainly helped by current knowledge from other areas such as graph theory, social networks, and informatics (Newman, 2010), whose network metrics are applied to study brain anatomy, its functional behaviour, and also the resilience against diseases.

Several techniques have been applied for brain network inference. Some of these are coherence (R), partial coherence, Granger causality (Granger, 1969), mostly applied as partial directed coherence (PDC) (Sameshima and Baccalá, 1999), synchronization likelihood (Stam and Dijk, 2002), phase coherence (PC) (Tass et al., 1998), imaginary part of coherency (ImCy) (Nolte et al., 2004), and phase lag index (PLI) (Stam et al., 2007).

In this paper we are interested in effects of the volume conduction problem on a recent synchronization measure for brain network inference, PLI. PLI is a technique designed to overcome the volume conduction problem, which causes techniques such as R and PC to favour close range connections due to the presence of neighbouring sources (Stam et al., 2007; Schoffelen and Gross, 2009; Nunez et al., 1997, 1999). Our simulations show that networks obtained by PLI present small-worldness due to high clustered nodes produced by volume conduction. This behaviour might lead to biased results in brain network inferences in EEG experiments if it is ignored.

Section 2 introduces brain networks and network measures, and R, PC and PLI are defined. Section 3 explains the volume conduction problem and its effects on synchronicity for bipolar recordings. In Section 4 we briefly explain the four sphere model. Our

* Corresponding authors. Tel.: +44 1904 322345.
E-mail addresses: luis.peraza@gmail.com (L.R. Peraza), david.halliday@york.ac.uk (D.M. Halliday).

0165-0270/$ – see front matter © 2012 Elsevier B.V. All rights reserved.
http://dx.doi.org/10.1016/j.jneumeth.2012.04.007

experiments are shown in Section 5 and our discussions on the results and conclusions are in Sections 6 and 7.

2. Brain networks

Brain neural network characteristics and properties are not completely understood yet. Nevertheless, technologies such as EEG, MEG, and fMRI, allow us to study the brain and search for its functional connectivity. In the case of the brain, small-world has been acknowledged as the topology of the brain's neural network and current research focuses on the understanding of the small-world brain (Sporns and Zwi, 2004).

2.1. Small world networks and metrics

In the seminal paper of Watts and Strogatz (1998), the small world network was quantitatively described for the first time. Before that, small world behaviour was already acknowledged in social networks but the manner to describe them and also to model their generation was unknown. For instance, it was known that social networks exhibited high clustering and short path length. High clustering is a feature of regular networks, networks that form symmetrical structures or lattice patterns by being connected with their closest neighbours. On the other hand, short path length which describes the number of edges among vertices, was a feature known for random networks. Small-world networks have a high clustering such as lattices but a short path length as random networks (Watts and Strogatz, 1998; Bassett and Bullmore, 2006; Newman, 2010). The path length is defined as

$$L = \frac{1}{n}\sum_{j\in N} L_j = \frac{1}{n}\sum_{j\in N}\frac{\sum_{k\in N, k\neq j} d_{jk}}{n-1}, \tag{1}$$

where d_{jk} is the number of steps (edges) between nodes j and k. Hence, L_j is the average distance between the node j and the rest of the network nodes. A problem in the path length measure L is that when one node is completely disconnected from the network, d_{jk} becomes undetermined and Eq. (1) is not valid. For disconnected networks there is another path length estimator called harmonic mean distance (Newman, 2010), defined by

$$L' = \left(\frac{1}{n}\sum_{j\in N}\frac{\sum_{k(\neq j)}(1/d_{jk})}{n-1}\right)^{-1}. \tag{2}$$

The clustering coefficient C is defined as

$$C = \frac{1}{n}\sum_{j\in N} C_j = \frac{1}{n}\sum_{j\in N}\frac{2t_j}{p_j(p_j-1)} \tag{3}$$

where

$$t_j = \frac{1}{2}\sum_{k,h\in N} a_{jk}a_{jh}a_{kh}, \tag{4}$$

$$p_j = \sum_{k\in N} a_{jk}, \tag{5}$$

where $a_{jk} = 1$ if there is an edge between nodes j and k, and $a_{jk} = 0$ if there is no connection between j and k. Eq. (5) is known as the node degree, the number of edges per node. The network average degree D is defined as

$$D = \frac{1}{N}\sum_{j\in N} p_j. \tag{6}$$

A concentrated measure for small-worldness is defined as

$$S = \frac{C/C_{rand}}{L/L_{rand}}. \tag{7}$$

Here C_{rand} and L_{rand} are the clustering and path length coefficients of a random network with equal number of nodes. $S \gg 1$ is indicative of small-worldness. For a review on these measures see Sporns and Zwi (2004), Newman (2010), and Rubinov and Sporns (2009).

2.2. Brain network inference

The searching of brain networks requires the design and study of brain network inference techniques. Several techniques have been applied for this task, among them are coherence, ImCy, PDC, PC, and PLI. Coherence itself defines a group of techniques that measure synchronization consistency between two or more time series. In this group of coherence techniques we can also find ImCy, PC, PLI and PDC. The latter one can be seen as parametric coherence, where an autoregressive (AR) model is used instead of the Fourier coefficients. There are practically two requirements to belong to this group of measures; to provide a measure for synchrony and to be bounded between 0 and 1, where 1 represents maximum consistency or completely dependent time series.

2.2.1. Coherence

Coherence can be seen as the spectral version of correlation. This measure is bounded between 0 and 1, this last one representing total dependence between both studied signals. Coherence is defined as

$$R_{jk}(\lambda) = \frac{|f_{jk}(\lambda)|^2}{f_{jj}(\lambda)f_{kk}(\lambda)}, \tag{8}$$

where $f_{jk}(\lambda)$ is the cross spectrum between time series j and k, and λ is the frequency index. If the modulus square is omitted in Eq. (8) the term is called coherency, which is a complex measure. Using coherency it is possible to infer causality between j and k by analysing the phase slope in complex coherency, see for instance Rosenberg et al. (1989) and Halliday et al. (1995). Causality can also be estimated by the imaginary part of Eq. (8) or ImCy, using the fact that ImCy can not be explained by instantaneous source interaction (see Nolte et al., 2004). Nevertheless, as explained in Stam et al. (2007), ImCy is affected by the amplitude of the sources and their phase delay, and in some cases it gives less useful results than standard coherence (Wheaton et al., 2005).

A coherence index R can be estimated by integrating Eq. (8) as

$$R_{jk} = \frac{1}{F}\int_{F\in\lambda} R_{jk}(\lambda)d\lambda \tag{9}$$

where F defines the frequency band. Eq. (9) is used to estimate EEG networks in our simulations. In this paper we use periodograms for the estimation of $f_{jk}(\lambda)$ using segments of 2^{10} samples with a square window, with no overlapping, and the FFT algorithm.

2.2.2. Phase coherence

Phase coherence (or PC) comes from the concept of phase locking or phase synchrony, see Tass et al. (1998) and Mormann et al. (2000). Here it is desired to measure if there is consistency between the phase difference of two time series, j and k. This difference is represented as

$$|\Delta\phi_{n,m}(t)| = |n\phi_j(t) - m\phi_k(t)| < const, \tag{10}$$

where n and m are integers, and $\phi_{j,k}$ are the phase of time series j and k. When this concept is applied to Neuroscience, we are interested in the isofrequency case, n and $m = 1$ (Tass et al., 1998; Quiroga et al., 2002). The difference in Eq. (10) becomes a stochastic variable on

the unit circle whose angle difference will tend to a constant value if both times series are synchronized. Using this phase difference consistency, PC is defined as

$$PC = \left| \frac{1}{M} \sum_{l=0}^{M-1} e^{i\Delta\phi(t_l)} \right|, \tag{11}$$

where we are using notation as in Stam et al. (2007) and M is the time series length. Since PC depends only on the phase difference, it is insensitive to the amplitude of both time series. The most used method to extract the instantaneous phase for PC is by using the analytical signal

$$x^H(t) = x(t) + i\tilde{x}(t), \tag{12}$$

where x^H is the analytical signal which is complex valued, $x(t)$ is the original time series, and $\tilde{x}(t)$ is its Hilbert transform. Hence, $x^H(t)$ can be represented as

$$x^H(t) = A(t)e^{i\phi(t)}, \tag{13}$$

where

$$A(t) = \sqrt{[x(t)]^2 + [\tilde{x}(t)]^2}, \tag{14}$$

and

$$\phi(t) = \arctan \frac{\tilde{x}(t)}{x(t)}. \tag{15}$$

2.2.3. Phase lag index

Phase lag index (or PLI) is another measure for phase consistency. PLI was proposed in Stam et al. (2007) as a measure for synchronicity which avoids the volume conduction problem (explained below) present in EEG. The logic of PLI is based on the fact that the imaginary part of coherency cannot be explained by volume conduction. In consequence the imaginary part reflects true interaction among different brain regions, and because it uses phase information only, PLI is also immune to the source amplitude problem (Guevara et al., 2005). Just as PC, PLI uses the phase difference in Eq. (10) to find phase consistency and it is defined by

$$PLI = \left| \frac{1}{M} \sum_{l=0}^{M-1} sign(\Delta\phi(t_l)) \right|. \tag{16}$$

Due to its close relation to PC, PLI can be represented as

$$PLI = \left| \frac{1}{M} \sum_{l=0}^{M-1} sign(Im(e^{i\Delta\phi(t_l)})) \right|. \tag{17}$$

By their constructions, PC and PLI are bounded measures between 0 and 1.

3. Volume conduction

The volume conduction problem in EEG results from the mixing of signals of neural origin caused by the conductive properties of the environment they propagate through. For EEG, the conductive properties of the brain, the cerebro spinal fluid (CSF), the skull, and the scalp cause a signal current generated by a neural source in the brain cortex to diffuse before reaching the scalp electrodes. Hence, a recorded time series using a scalp electrode is not necessarily generated by a source below it.

Volume conduction produces an instant (zero lag) correlation among sources, and it is represented commonly as a linear mixture of the brain sources $\mathbf{S}$ as

$$\mathbf{X} = \mathbf{HS}\ , \tag{18}$$

where $\mathbf{X} = [x_1(t) \ldots x_N(t)]^T$, $\mathbf{S}$ is a column matrix with the source time series $s_n(t)$, and $\mathbf{H}$ is the mixing matrix that describes the behaviour of the conductive environment. Common techniques that deal with volume conduction rely on the solution of the inverse problem, these techniques aim to unmix the source signals in Eq. (18) by estimating $\mathbf{H}$. In this paper we are not dealing with the inverse problem since in our simulations we are assuming that the real sources are known and also their position, which is exactly below the EEG electrodes. For a review on this topic see Nunez and Srinivasan (2006).

3.1. Volume conduction and synchronicity

Volume conduction might affect the output of synchronization measures when using EEG signals, because EEG is bipolar by nature. This means that EEG signals are composed of a difference between an electrode of interest and a reference. Guevara et al. (2005) discuss this issue when using bipolar signals and synchronicity measures. The straight forward approach to deal with this problem in EEG is by referencing digitally the EEG montage. In our simulations we used electrode averaging (Nunez and Srinivasan, 2006) because this is the most common reference method applied in clinical EEG. Recalling Eq. (18) and assuming a common reference, *ref*, we can represent the acquired set of bipolar signals $\mathbf{X}_B$ as

$$\mathbf{X}_B = \mathbf{X} - ref\ . \tag{19}$$

Subtracting the averaged bipolar signals we have that

$$\begin{aligned} \mathbf{X}_A &= \mathbf{X} - ref - \frac{1}{N}\sum_{n=1}^{N} x_{Bn}(t) \\ &= \mathbf{X} - \frac{1}{N}\sum_{n=1}^{N} x_n(t), \end{aligned} \tag{20}$$

where $\mathbf{X}_A$ is the acquired EEG using average reference. Eq. (20) shows that in theory, when performing average reference in EEG we are only dealing with volume conduction and solving in part the bipolar synchrony problem mentioned in Guevara et al. (2005). Therefore, two independent neural sources, $x_j(t)$ and $x_k(t)$, will have instant relation due to the volume conduction problem.

If we define three time series $s(t)$, $x(t)$, and $y(t)$ where $s(t) = x(t) + y(t)$, compute their analytic signals ($s^H(t)$, $x^H(t)$, $y^H(t)$) using the Hilbert transform to obtain $s^H(t) = s(t) + i\tilde{s}(t)$ where $\tilde{s}$ is the Hilbert transform of s and the same applies for $x(t)$ and $y(t)$, we can obtain instant phase. Then, we compute the relative phases of $s(t)$ and $y(t)$ with respect to $x(t)$ (this is equivalent to zeroing out the phase of $x^H(t)$) leading to

$$\sin\phi_s = \frac{\tilde{y}(t)}{|s^H(t)|} \quad \text{and} \quad \sin\phi_y = \frac{\tilde{y}(t)}{|y^H(t)|}\ , \tag{21}$$

where $|s^H(t)|$ and $|y^H(t)|$ represent magnitude values. Eq. (21) is valid for the range $0 \le \phi_y \le \pi/2$, from which we can see that $|s^H(t)| \ge |y^H(t)|$. Hence

$$\sin\phi_s \le \sin\phi_y \quad \text{or} \quad \phi_s(t) \le \phi_y(t). \tag{22}$$

Subtracting ϕ_x from both sides of the inequality, we have that

$$\begin{aligned} \phi_s - \phi_x &\le \phi_y - \phi_x, \\ \Delta sx(t) &\le \Delta yx(t). \end{aligned} \tag{23}$$

Notice that Eq. (23) holds for all the complex plane, but for negative phase differences we have to use absolute values $|\Delta sx(t)| \le |\Delta yx(t)|$. In consequence, we are able to state that the phase difference of two linearly dependent signals is always lower than the phase difference of their unmixed independent elements

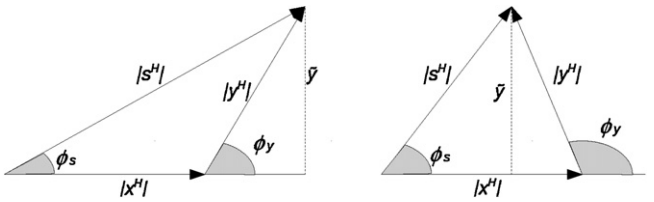

Fig. 1. Analytic phasors of two correlated signals $s(t)$ and $y(t)$ on the complex plane. The figure shows that $\phi_s(t)$ is always lower than $\phi_y(t)$, being the phase angles of $s(t)$ and $y(t)$, respectively.

regardless of their magnitude (equality holds when $x(t) = 0$). For a visual reference see Fig. 1.

The distributions of ϕ_y and ϕ_x are uniform from $-\pi$ to π, this makes Δyx distribution triangular from -2π to 2π (uniform from $-\pi$ to π). Nevertheless, the Δsx phase distribution will be more centred around 0 due to Eq. (23). Fig. 2 shows these scenarios in the first and third column for the correlated and independent cases, respectively.

Now, assume that we have a fourth independent signal $z(t)$ and we want to know how $\Delta yz(t)$ relates to $\Delta yx(t)$ and $\Delta sx(t)$. $\Delta yz(t)$ will have a probability distribution equal to $\Delta yx(t)$, thus we can say that both phase differences are statistically equivalent. Furthermore $\Delta sx(t)$ has a more centred distribution than $\Delta yx(t)$, and in consequence more centred than $\Delta yz(t)$. Therefore, we can state that $\Delta sx(t)$ is lower in probability than $\Delta yz(t)$. In other words, if we sample at any instant t $\Delta yz(t)$, it will be most of the cases higher than samples obtained from $\Delta sx(t)$. We can represent this as

$$\begin{aligned} p(|\Delta yz(t)| < \theta) &= p(|\Delta yx(t)| < \theta) \\ p(|\Delta yz(t)| < \theta) &< p(|\Delta sx(t)| < \theta) \end{aligned} \tag{24}$$

where θ is a constant between 0 and π. Notice that techniques like coherence and PC are highly affected by Eqs. (23) and (24), while

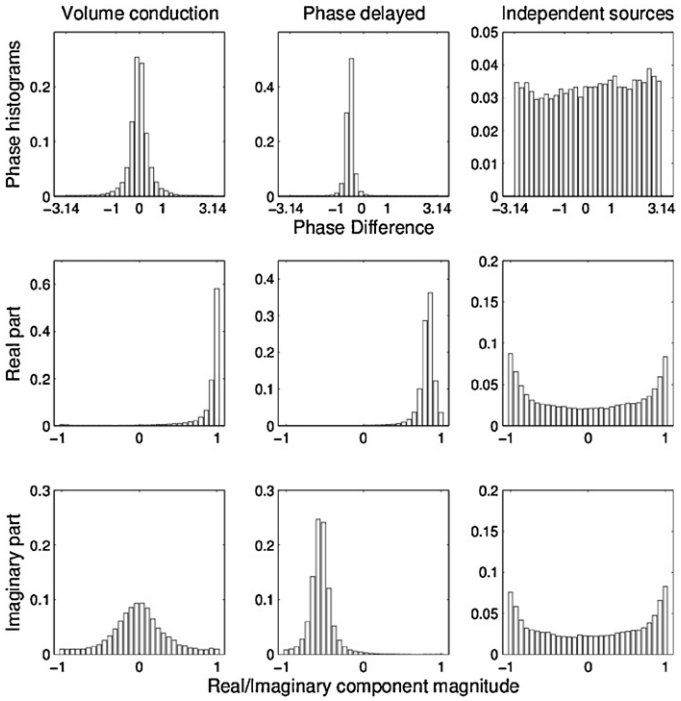

Fig. 2. Histograms for different cases of phase difference estimation using the analytic signal. The first column shows the case of two mixed signals with zero lag, the middle column a true delayed interaction and the third column shows phase difference histograms for independent time series. The second and third row show histograms for the real and imaginary part of the analytic signal for the three cases.

PLI is invariant to this cross mixing. We can see this from Eqs. (23) and (16), since

$$PLI[\Delta sx(t)] = PLI[\Delta yx(t)]. \tag{25}$$

Nevertheless, we show that PLI is affected by the cross mixing and the influence of multiple sources.

4. Methods

In this section we explain the framework to develop our experiments. In order to simulate EEG recordings as close as possible to a real EEG test, we implemented the four sphere model for volume conduction (Nunez and Srinivasan, 2006). The four sphere model allows to simulate the interaction among different sources at cortical level and measure their potential at scalp level.

4.1. Volume conduction model

We simulate volume conduction in the human head using the four sphere model described in Nunez and Srinivasan (2006). The model consists of four concentric spheres representing the brain, CSF, the skull, and the scalp skin. The conductivity ratios of the four tissues are $\sigma_1/\sigma_2 = 0.2$, $\sigma_1/\sigma_3 = 40$, $\sigma_1/\sigma_4 = 1$. The radii of the spheres from r_1 to r_4 are 8, 8.1, 8.6 and 9.2 cm as shown in Fig. 3a.

Fig. 3b shows the acquisition simulation with the 64 electrodes on the spherical head scalp. The figure also shows the voltage distribution of a radial source below electrode F6. 64 radial sources were placed below each electrode at 7.5 cm from the spheres' centre, and their activity were modulated by independent AR processes whose coefficients were estimated from real EEG recordings.

4.2. EEG modelling

We create synthesized brain signals using an AR model (see Hayes, 1996) whose coefficients were estimated from real time series from an EEG experiment published in Halliday et al. (1998). Using the AR coefficients we are able to generate infinite sets of synthesized EEG signal segments while preserving the spectral properties of real brain time series. In Halliday et al. (1998), EEG recordings were made over the sensorimotor cortex at 1000 Hz sampling rate. For our simulations we downsampled these recordings to change the sampling rate to 500 Hz. We choose one clean segment in order to avoid artifacts and this was modelled with an AR model of order 10. Sets of 64 independent brain sources were synthesized after throwing away the first 2000 generated samples.

4.3. EEG electrode montage

We use the Biosemi EEG 64-electrode layout available at http://www.biosemi.com. In order to simplify our experiments, we locate the simulated brain sources below each of the 64 available electrodes. Hence, in our experiments we measure the interaction among 64 independent brain sources.

5. Experiments

In this section we test PLI for network inference in two experiments. First the performance of PLI when estimating synchronicity between two independent and two linearly mixed sources is tested. This experiment aims to prove that PLI is invariant to linear mixing, and see if its statistical behaviour is similar for the independent and correlated cases. For the second experiment we implement an EEG test simulation using the four sphere head model and 64 sources located in the brain. This simulation will allow to test PLI

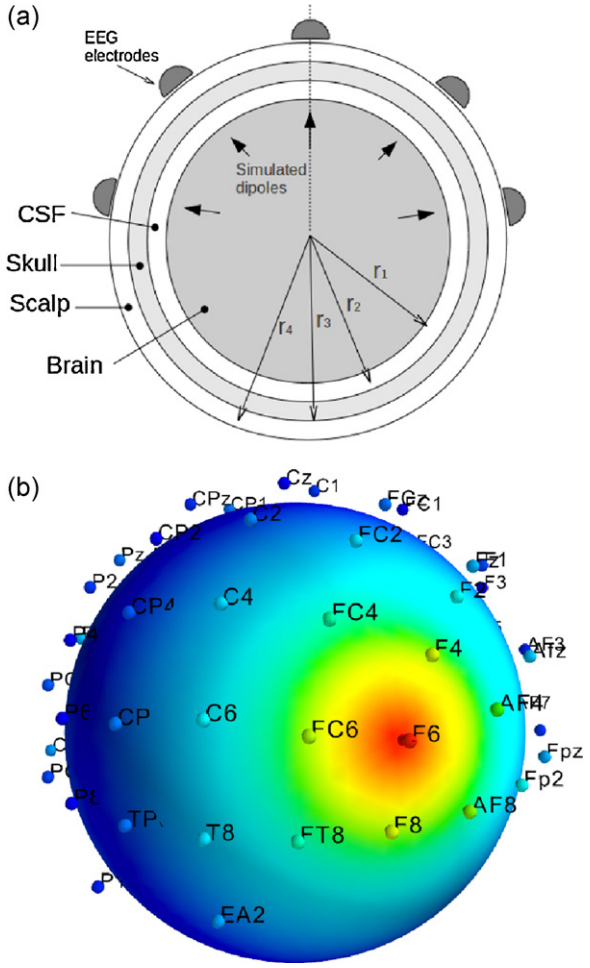

Fig. 3. The four sphere head model. (a) The model is composed of four concentric spheres representing from the inner one to the outer; the brain, CSF, the skull, and the scalp (image adapted from Nunez and Srinivasan, 2006). Also, a schematic view of the EEG acquisition simulation is shown. Electrodes were arranged according to the Biosemi EEG 64 electrode layout (http://www.biosemi.com) and the brain sources were located below each electrode. (b) EEG acquisition simulation using the four sphere model with the 64 electrodes plus 2 references placed on the scalp. The figure shows the voltage distribution of an activated brain source located below electrode F6.

behaviour when several independent sources are interacting in an environment affected by volume conduction.

5.1. Correlated and independent sources

For the first experiment we calculate PLI for two pairs of time series x_1, x_2 and x_1, x_3. x_1 and x_3 are related by the mixing equation

$$\begin{bmatrix} x_1 \\ x_3 \end{bmatrix} = \begin{bmatrix} a & b \\ b & a \end{bmatrix} \begin{bmatrix} y_1 \\ y_3 \end{bmatrix} \tag{26}$$

where $0 \leq a \leq 0.5$ and $b = 1 - a$. a and b are constants that vary the level of interaction from independent to full correlated sources, and y_1, y_3 and x_2 are independent EEG signal sources modelled as explained in Section 4.2, and filtered at the alpha band (8–12 Hz) to obtain narrower spectrum. Here we want to measure PLI for (x_1, x_2) or PLI_{12} and PLI_{13} with no delay.

In the first case we are testing the null hypothesis, where we know in advance that no interaction exists between x_1 and x_2 (PLI_{12}), and in the second case we are measuring a true interaction with no delay (PLI_{13}).

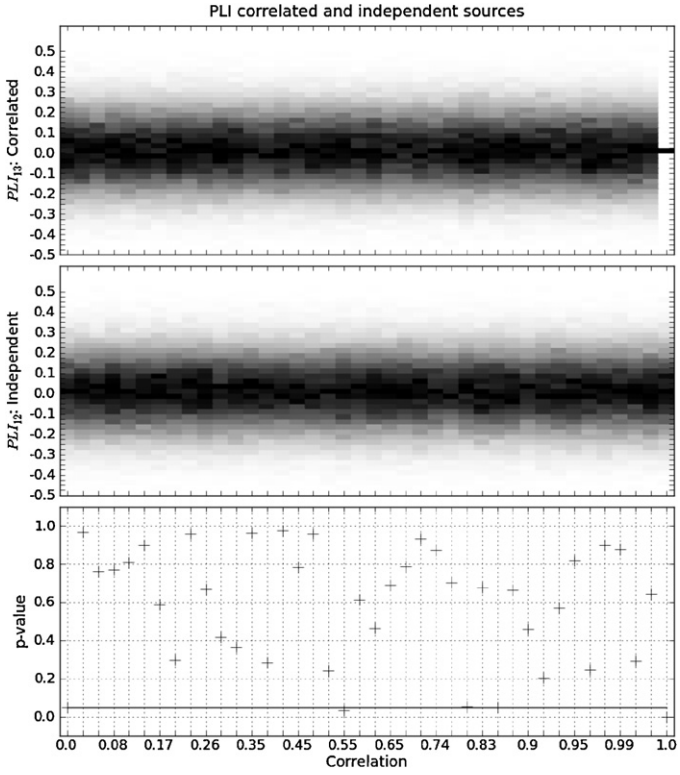

Fig. 4. PLI estimation between correlated and independent sources. PLI_{13} (top) shows PLI estimation between two dependent signals, whose correlation is defined by the mixing matrix in Eq. (26) and shown in the x-axis. The graph shows 40 histograms arranged in columns, all of them centred at zero approximately and having similar shape distribution. The only remarkable difference is achieved when ρ_{13} reaches one, when PLI gives only zeros. The middle graph also shows 40 histograms arranged in columns for PLI_{12} estimations between two fully independent signals. The bottom graph shows p-values from the non-parametric permutation test (5000 permutations) between histograms in PLI_{13} and PLI_{12}. If the p-value surpasses the significance criterion (p-value= 0.05 and marked with an horizontal line), we say that both histograms were created using samples taken from the same process.

Fig. 4-top shows the PLI results for PLI_{13}. Here a consists of 40 values linearly spaced and varying from 0 to 0.5 to create different levels of correlation according to Eq. (26). The correlation coefficient between x_1 and x_3 is defined by $\rho_{13} = 2ab/(a^2 + b^2)$.

Each column in Fig. 4-top shows the normalized histograms of 5000 PLI_{13} estimates using time series of 5000 samples for 40 correlation levels from 0 to 1 as defined in Eq. (26). As expected, PLI_{13} is invariant to different levels of correlations giving very low PLI values, and the sample distributions show similar shape through all correlation levels. The only remarkable difference is found when the correlation level reaches $\rho_{13} = 1$, at which PLI_{13} gives only zeros, indicating full synchronicity. These results agrees with Eq. (25) which refers to the correlation invariant property of PLI.

Fig. 4-middle row shows the results for PLI estimations between two independent sources (PLI_{12}). The computations are the same as in Fig. 4-top for PLI_{13}. PLI_{12} estimations show similar results to PLI_{13}, the histograms peak around 0 and their shapes remain similar. In this case similar distribution shapes was expected since all estimations were taken from independent sources.

To test the equivalence between PLI_{13} and PLI_{12} we use the non-parametric permutation (NP) test (Nichols and Holmes, 2002) using 5000 permutations. The NP test aims to find if two datasets were sampled from the same distribution, in this case the null hypothesis. If the NP p-value results higher than the chosen significance threshold, the null hypothesis cannot be rejected. Fig. 4-bottom shows 40 p-value outcomes from the NP test between PLI_{13} and PLI_{12} sample distributions. The level of significance chosen was 0.05

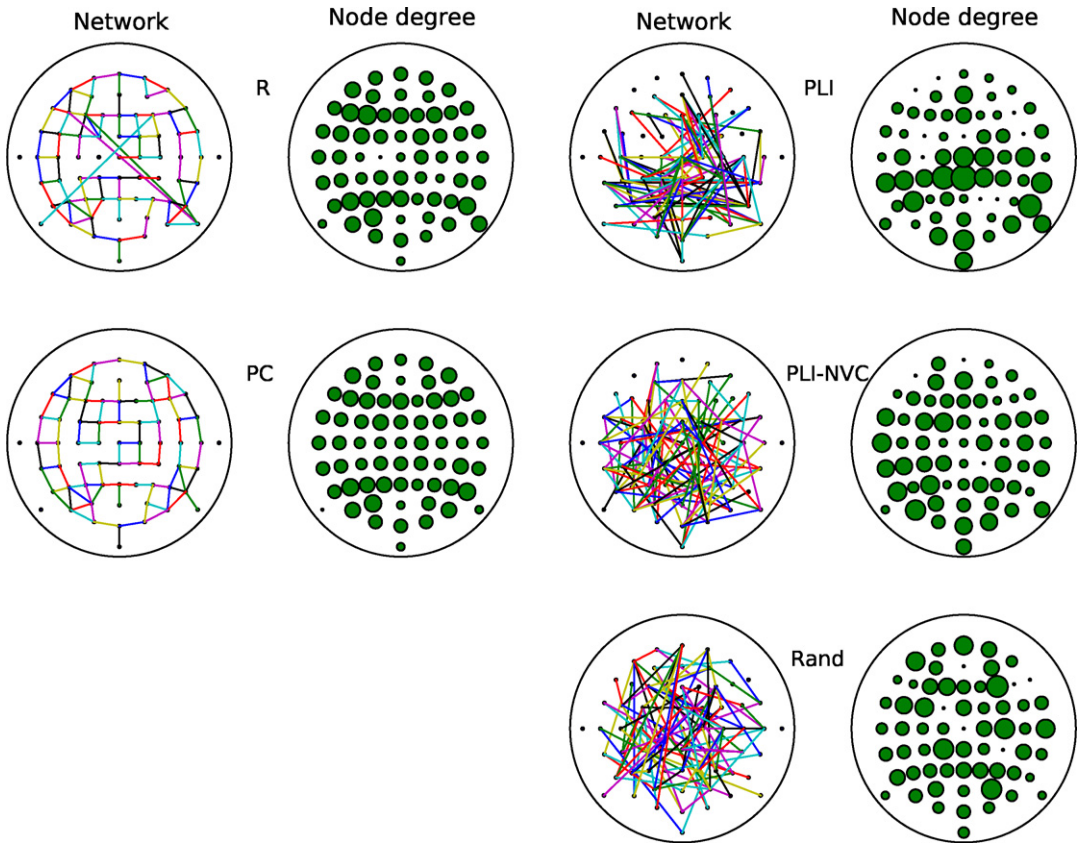

Fig. 5. Single experiment of simulated EEG acquisition using uncorrelated sources, volume conduction and inference of networks using coherence (R), phase coherence (PC), and phase lag index (PLI). The results for every estimator (R, PC, and PLI) are shown in pairs; the estimated network and the degree plot. The former shows estimated scalp networks using the synchronicity measures, where in all cases the chosen average network degree is $D = 3$. The degree plot shows the node degree (the number of edges) of every electrode. Here the size of the circles are proportional to the degree at their location. Network results for random (Rand) and PLI-NVC (NVC stands for no volume conduction) are also shown. Random network's edges were chosen with uniform distribution until an average degree of 3 was obtained. PLI-NVC was obtained by estimating PLI values among the original sources before volume conduction. Notice that PLI obtains networks that resemble at first glance a random network, but the edge degree of some of its nodes is higher than expected.

which is marked with a horizontal line. As can be seen, both distributions passed the NP test at all correlation levels, with exception of $\rho = 1$ which gave a p-value=0.0 and $\rho = 0.55$ which is the only value below the threshold produced by the variability of the distributions.

These results agree with Eq. (24) (first row), which refers to the equality in probability distributions of independent sources. Fig. 4 shows that PLI is invariant to zero lag correlation.

5.2. EEG acquisition simulation

For the second experiment, 64 independent brain sources were placed in the four sphere head model at the level of the brain cortex, a radius of 7.5 cm. The sources' time series were modelled as explained in Section 4.2 generating segments of 5120 samples (5×2^{10} plus 2000 samples that are discarded after filtering). The time series were filtered at Theta (4–8 Hz), Alpha (8–12 Hz), Beta 1 (12–20 Hz), Beta 2 (21–29 Hz), Gamma 1 (30–35 Hz) and Gamma 2 (35-40 Hz). This section shows the results for the alpha band only, since the other bands gave similar results. Nevertheless, statistical significance tests using the NP test (see Section 5.1) are shown for the six defined frequency bands.

The position of the modelled sources is exactly below the EEG scalp electrodes which were placed at positions defined by the 64-electrode Biosemi's layout, see Fig. 3. The implementation of the four sphere model allows to obtain the matrix $\mathbf{H}$ in Eq. (18) that performs the source mixing in Eq. (20), according to the volume conduction model, the positions of the sources, and the scalp electrodes. For plotting purposes, the distance among electrodes is shown normalized for a sphere of unit radius.

Fig. 5 shows a single experiment of network estimation for R, PC and PLI under the null hypothesis whose networks were thresholded (an edge was set to 1 if it was above the threshold and deleted otherwise) for an average network degree $D = 3$ in all cases. Furthermore, in order to compare the networks obtained under the null hypothesis, we also compute a random network, where the edges were connected among the nodes with uniform distribution until a $D = 3$ was obtained. Finally, we estimated networks without the volume conduction effect, PLI-NVC (where NVC stands for no volume conduction), R-NVC and PC-NVC, using the original modelled brain sources at the cortical level under the same criterion for D.

It can be seen in Fig. 5 that PLI gives a network similar to a random network but some of the nodes show high clustering. Since it is assumed that PLI is invariant to volume conduction, it is expected that the edges found in a network experiment under the null hypothesis will be at least similar to a random network, as it occurs for PLI-NVC. Nevertheless, the null network found by PLI under volume conduction is different from random. This suggests that PLI is affected by volume conduction in this case. In Fig. 5, $D = 3$ was chosen as example because this degree value offers a network density that allows to observe the network behaviour more easily (see PLI case in Fig. 5). Higher values of D will show cluttered networks that obscure the purpose of the figure.

In order to study the behaviour of PLI in network inference we repeated the previous experiment 500 times, for different average network degrees from $D = 2$ to $D = 32$. Varying the edge threshold

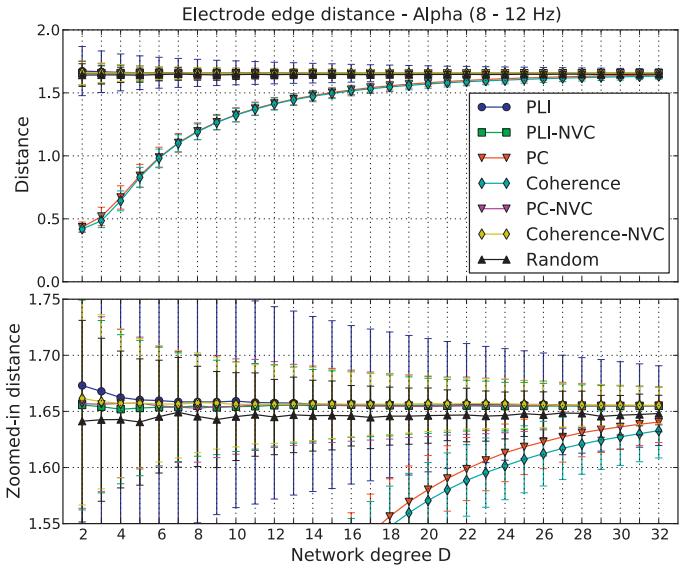

Fig. 6. Results of 500 iterations of the experiment shown in Fig. 5 for multiple average degree values from $D=2$ to $D=32$. The figure shows the average edge distance (y-axis) among electrodes on a normalized sphere (radius 1) versus the average node degree D (x-axis). The standard deviation at every degree is also shown as error intervals. Notice that the distance for PLI, PLI-NVC and Random networks are similar through all degree cases. Bottom graph shows a zoom of the top graph. This result shows that PLI does not favour close range connections as PC and R do due to volume conduction and as can be observed in the PC and R curves. NVC stands for the no volume conduction case.

while maintaining the network degree fixed is a common practice for network comparison, see for instance Micheloyannis et al. (2009), Sporns and Zwi (2004), and Milo et al. (2002). An equivalent approach is to take only the strongest P number of connections since $P = D \times N/2$ (De Vico Fallani et al., 2009). All experiments were performed for the six frequency bands defined above. Figs. 6–8 show results for the Alpha band.

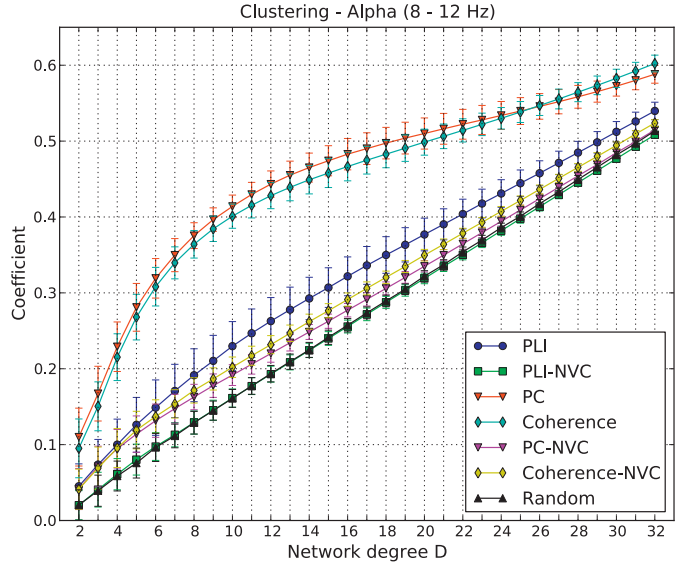

Fig. 7. Clustering coefficient versus average node degree curves. The figure shows the clustering coefficient value of EEG networks using PLI, R, PC and their no volume conduction (NVC) cases, through different average node degrees from $D=2$ to $D=32$. As expected random networks show a low coefficient while PC and R gave a high coefficient. PLI obtained clustering not as high as PC and R, but significantly higher than random networks and PLI-NVC. The difference in the curves of PLI and PLI-NVC suggest that volume conduction influence the PLI edge estimation performance.

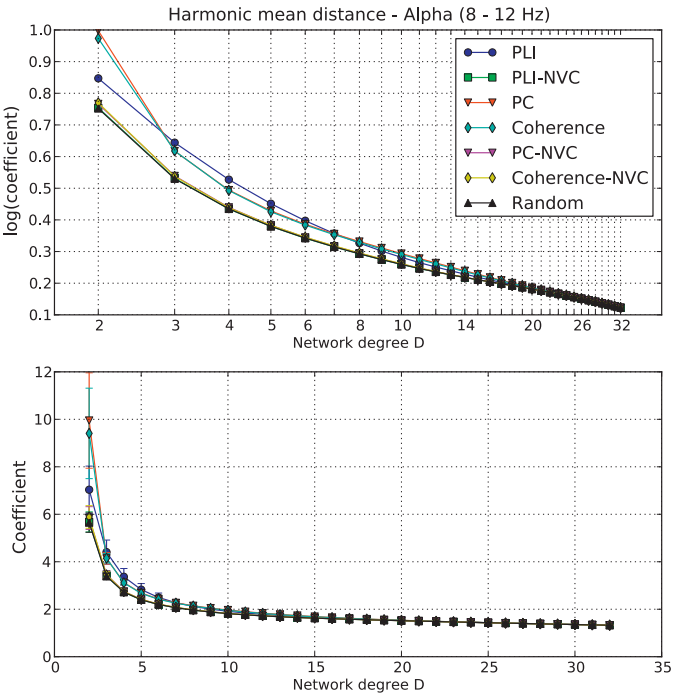

Fig. 8. Harmonic mean for the same experiments in Figs. 6 and 7. The harmonic mean shows an estimate for the path length in networks that have disconnected nodes. There are two curve crossings between PLI and PC-Coherence, the first one between $D=2$ and $D=3$, and the second one between $D=7$ and $D=8$. PLI-NVC and Random show similar values. As the average node degree increases, all coefficients tend to a common value.

Fig. 6 shows curves of the edge length between electrodes (nodes), this means the physical distance over the spherical scalp among connected electrodes. Notice that PLI and PLI-NVC curve trajectories are similar to random networks, practically constant among the different network degrees, around 1.65. Also, the average edge length trajectories of curves R and PC are similar. At the lowest degree, $D=2$, it is just above 0.4 (the minimum normalized distance between two electrodes for the Biosemi EEG layout is 0.32). As the average degree grows, the electrode edge distance tends to values close to random networks due to the network edge cluttering. For R-NVC and PC-NVC, the edge length follows random network behaviour. This was expected since R and PC are being computed between independent sources.

Fig. 7 shows the results for the clustering coefficient. As expected R and PC gave high clustering values compared to random networks. PLI showed a clustering coefficient above Random and PLI-NVC, these two follow similar trajectories. R-NVC and PC-NVC show also values above Random, even though R and PC are being computed for independent sources. R and PC are also affected by the length of the time series and their amplitudes besides volume conduction. We discuss this in Section 6.

Because the estimated networks are highly disconnected, it is impossible to compute the path length metrics as commonly defined. Instead, we used the harmonic mean distance (Eq. (2)) commonly applied in network analysis to obtain an estimate for the path length ignoring the disconnected nodes whose paths are undetermined. Fig. 8-top shows the results for the harmonic mean distance results in a log_{10}–log_{10} scale for better visibility. There are two crossings between R and PLI, the first between $D=2$ and $D=3$ and the second between $D=7$ and $D=8$. In all cases PLI showed a higher harmonic distance than Random and PLI-NVC, these latter ones showing similar values and the same for R-NVC and PC-NVC.

Since PLI networks under the null hypothesis resembles at first glance a random network (see Fig. 5 for a visual example), the

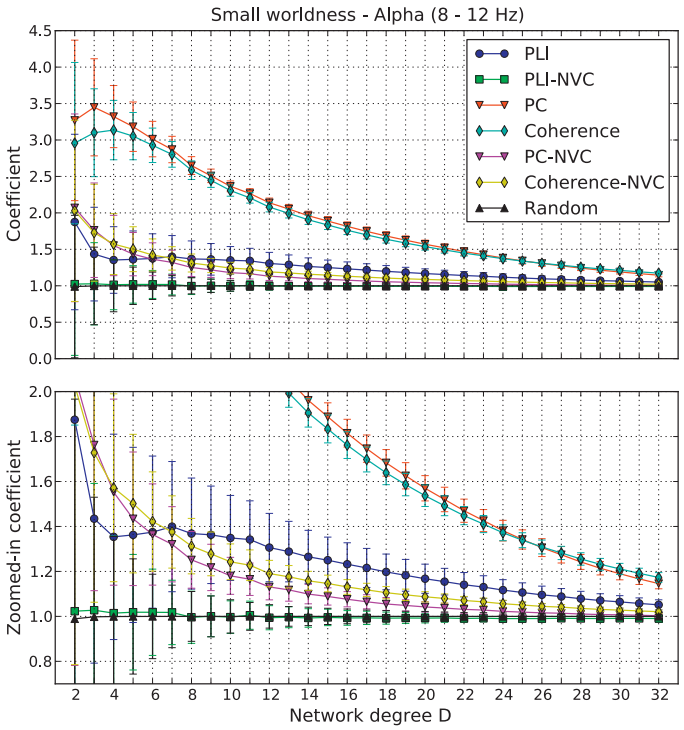

Fig. 9. Using previous results, we compute small-worldness S for all experiments. Networks obtained by PLI show in all cases higher small-worldness than PLI-NVC and random networks. Although S indices obtained by PLI are not much higher than 1 as it is for PC and R. It is still significantly higher than the random network cases. Bottom graph shows a zoom of the top graph.

harmonic mean values were expected to be in the range of a random network, but instead of that their values are higher.

Finally, using the previous results we compute the small-worldness index using the clustering coefficients and the harmonic distance means of random networks as normalizing factors. The results for the 500 experiments are shown in Fig. 9 for all network degree cases. Again, small-worldness was expected for PC and R, since this is common for grid networks produced by the sensitivity of PC and R to volume conduction. For random networks, the mean is exactly 1 and PLI-NVC in Fig. 9 is close to 1. In network analysis a small-worldness index much higher than 1 is considered an indicator of a small-world, and PLI shows clearly a small-world index above one for networks that do not resemble a grid but a random network. R-NVC and PC-NVC also show small-worldness due to the clustering in these networks, see Fig. 7.

5.2.1. Statistical comparisons

In order to measure the differences between PLI, PLI-NVC inferred networks and random networks, we use the NP test. For these experiments we estimate 10, 000 networks per each network degree from $D = 2$ to $D = 32$ and the NP tests were computed using 10, 000 permutations (Nichols and Holmes, 2002). NP p-values for network metrics between the sample population pairs Random-PLI-NVC and Random-PLI are computed for six frequency bands: Theta (4–8 Hz), Alpha (8–12 Hz), Beta 1 (12–20 Hz), Beta 2 (21–29 Hz), Gamma 1 (30–35 Hz), and Gamma 2 (35–40 Hz). The first pair (Random-PLI-NVC) aims to test the statistical differences between Random networks and networks inferred using PLI with no volume conduction. Random-PLI sees if networks inferred using PLI under volume conduction differ from random networks.

Fig. 10 shows the NP p-values for the small-world simulation between Random and PLI-NVC inferred networks. We hypothesized that networks inferred using PLI-NVC under the null

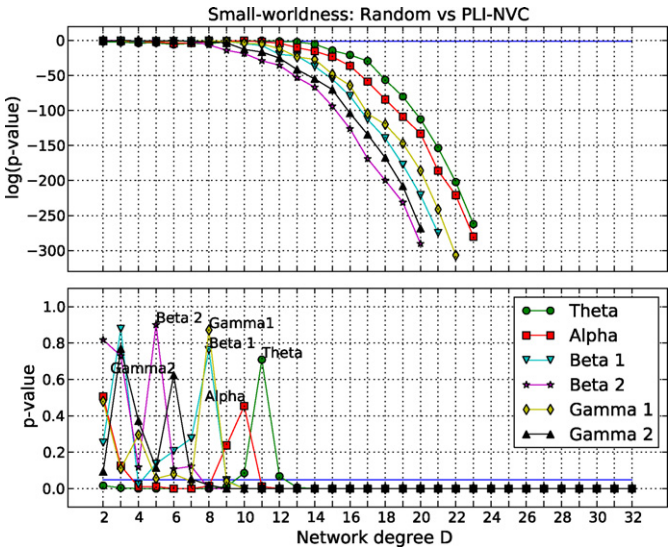

Fig. 10. Non-parametric permutation (NP) test between PLI-NVC and Random small-world using 10, 000 network estimations and 10, 000 permutations for the NP test. The chosen significance threshold p-value is 0.05 shown with a horizontal line. The NP p-values at the bottom graph show important peaks where the small-world means of Random and PLI-NVC intersect; Theta at $D = 11$, Alpha at $D = 10$, Beta 1 at $D = 8$, Beta 2 at $D = 5$, Gamma 1 at $D = 8$, and Gamma 2 at $D = 6$. Top graph shows p-values with a logarithmic ($\log_{10}$) scale for the y-axis. Bottom graph shows the same results in a linear scale.

hypothesis (independent sources) should present a random topology. Fig. 10 shows that this is not true. Although PLI-NVC is very close in all their network measures to Random networks, the NP test for the small-world metrics shows that there are significant differences between both topologies at a significance level of 0.05. Small-world curves in Fig. 13 for PLI-NVC and Random show that these curves are very close and their means intersect at $D = 10$ in this case for the Alpha band. The other bands also show crossovers at different degrees; Theta at $D = 11$, Beta 1 at $D = 8$, Beta 2 at $D = 5$, Gamma 1 at $D = 8$, and Gamma 2 at $D = 6$. These curves' crossovers between the small-world means of PLI-NVC and Random produce large p-value peaks as shown in Fig. 10. Large p-values at lower degrees ($D = 2 - 4$) are produced by the small-world variance. As the network degree increases, the small-world variance decreases highlighting the difference between PLI-NVC and Random small-worldness.

Fig. 11 shows the same tests but for PLI when it is affected by volume conduction, PLI-VC. All p-values were 0.0, which indicates that

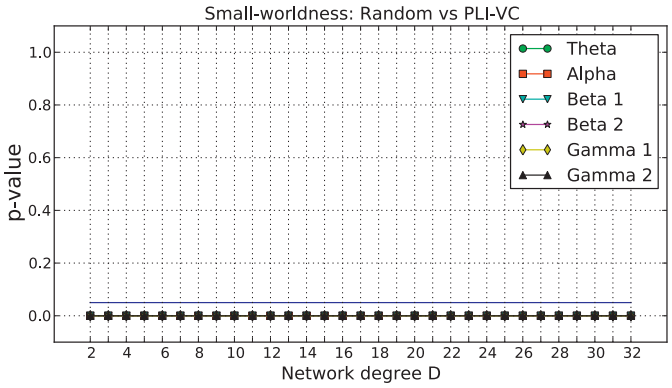

Fig. 11. Non-parametric permutation (NP) test between PLI and Random small-world network using 10, 000 network estimations and 10, 000 permutations for the NP test. The significance threshold is shown with a horizontal line at p-value=0.05. In this plot all NP p-values are 0.0.

we cannot say that both distributions are similar at all frequency bands and network degrees.

The difference between PLI-NVC and Random networks is mainly governed by the clustering coefficient. This is shown in Fig. 12 where the p-values show similar behaviour to the ones in Fig. 10. The curves' intersections between PLI-NVC and Random clustering produces a p-value peak per each frequency band as labelled in the bottom graph. High p-values at lower degrees ($D = 2-4$) occur because the clustering variance is large at these degree values.

Using experimental setup in Section 5.2, we created PLI histograms for the $N(N-1)/2$ possible EEG electrode edge connections in the Alpha band. This allows the estimation of the probability distribution of the null hypothesis taking into account the volume conduction effect. Fig. 14 aims to show similar phenomenon to Fig. 4 for the invariance of PLI to zero-lag correlation, but here we are showing the standard deviations of PLI estimates taken from independent sources in a volume conduction environment.

Fig. 14 shows the standard deviations of 10,000 PLI estimates for the $N(N-1)/2$ possible connections using PLI and PLI-NVC. The lower triangular matrix shows the case for volume conduction while the upper triangular part shows the standard deviations for PLI-NVC. Notice that the upper triangular matrix has higher values than the lower part. This indicates that PLI when affected by volume conduction tends to be closer to zero than the NVC case.

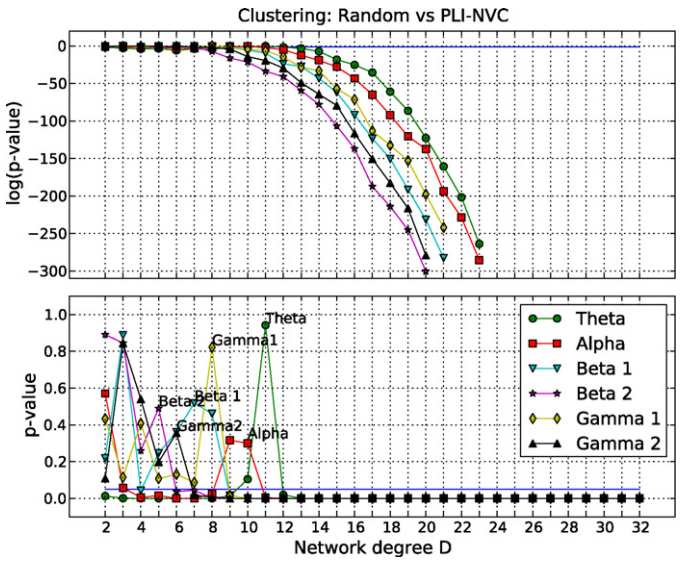

Fig. 12. Similar test than in Figs. 10 and 11 but for the clustering coefficient estimator. Top graph shows p-values in a logarithmic $\log_{10}$ scale for the y-axis. Bottom graph shows the same results in a linear scale.

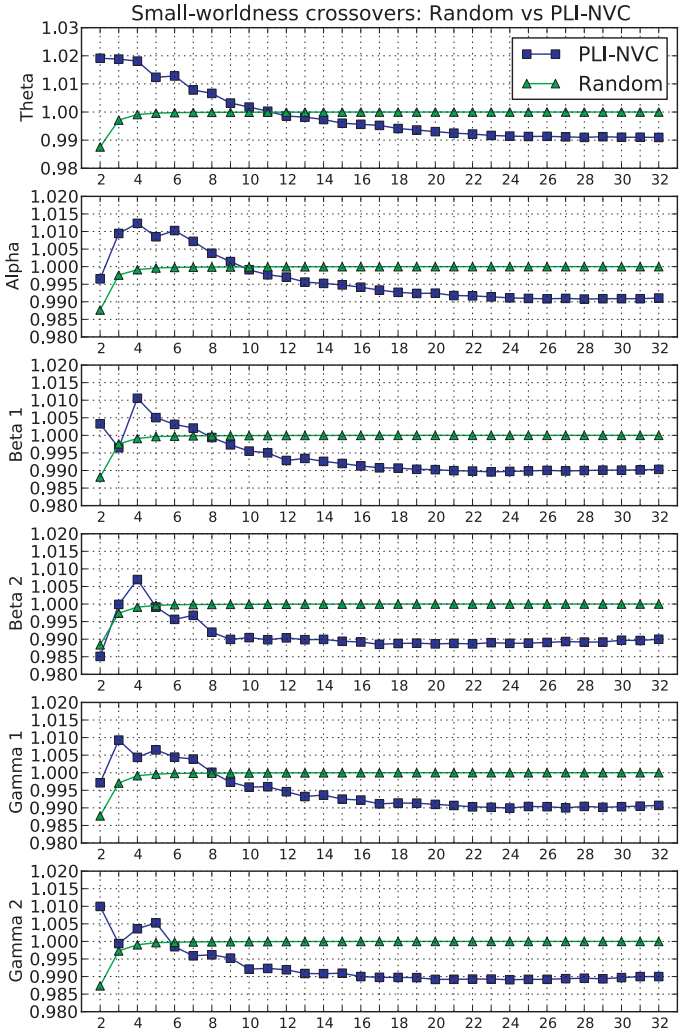

Fig. 13. Small-world mean crossovers. The figure shows the small-world means of the 10,000 network estimation experiments for the pairs PLI-NVC and Random network at the analysed frequency bands: Theta, Alpha, Beta 1, Beta 2, Gamma 1, and Gamma 2. Notice the the NP p-values peaks in Fig. 10 correspond to the graph intersections.

6. Discussion

We tested the performance of a well known edge estimation technique, PLI, widely applied for network estimation in EEG. Other techniques like coherence and PC are well documented in the literature (see for instance Nunez et al., 1997, 1999; Guevara et al., 2005; Stam et al., 2007). Coherence and PC obtain networks that resemble a grid due to the volume conduction problem which favours close range connections. To overcome the volume conduction problem, PLI was proposed in Stam et al. (2007) as a variant of PC that takes into account the phase difference sign only.

The results in Fig. 4 show an interesting property of PLI when working with correlated and independent time series. PLI gives similar values for zero-lag correlated signals and also for independent signals. This is a favourable behaviour for PLI since it is desired to ignore the zero-lag mixing between sources, and at least when only two sources are involved, the PLI correlation invariant property holds. Nevertheless, our simulations suggest that when more sources are involved, PLI is affected by the sources' interaction.

We used the four sphere model to simulate EEG acquisition. Then we placed 64 independent EEG sources at brain level. This implementation gave us access to the 64 brain sources and also to the 64 electrode EEG recordings, which represent the activity of the original sources after volume conduction. Our original hypothesis was that if PLI is invariant to volume conduction as normally stated, the PLI networks found in source domain should be similar to the ones found in the electrode domain. Our simulations showed that this is not the case. The networks at the electrode level are significantly different to the ones found at the source level, proving that volume conduction affects PLI network estimation when working with multiple sources.

Furthermore, our results show that although the networks inferred using PLI-NVC and Random networks are very similar as shown in Figs. 7 and 9, they are statistically different. The small-world PLI-NVC curves produced by the analysed frequency bands intersect the small-world Random curve, see Fig. 13. These crossovers produce large p-value peaks as can be seen in in Fig. 10-bottom. PLI-NVC inferred networks differ statistically from Random but they are still very close to this topology, and closer than R-NVC and PC-NVC proving that PLI is more robust than these techniques.

The higher variability of the network measures (clustering, harmonic mean distance, and small-worldness) at low average network degrees is because at these degrees there is a larger universe of network structures that can be built due to the "free" node pairs where an edge can be placed. As the average degree increases and in consequence the number of edges, the number of network structures that can be built decreases, which means that there are less variability for the networks and lower variance in all network measures.

The main characteristic of PLI networks when affected by volume conduction are their high clustering coefficient compared to random networks. Since PLI-NVC networks did not show high clustering we can state that high clustering in PLI was produced by volume conduction, which also causes small-worldness as we showed in Fig. 9. The clustered nodes produce a second characteristic for PLI estimated networks, their high harmonic mean distance. High clustered nodes produce long paths when several of these nodes make contact through their edges.

There is also an interesting behaviour of PLI under volume conduction shown in the standard deviation matrix (lower triangular part) in Fig. 14. The PLI distributions of the $N(N-1)/2$ possible connections have lower standard deviations than PLI-NVC. This indicates that volume conduction affects PLI by narrowing its distribution when several sources interact. This result is against the PLI invariant property to zero-lag correlation shown in Fig. 4 and suggests that when PLI is affected by several spurious sources its correlation invariant property cancels. Nevertheless, as we mention previously PLI is more robust than coherence and PC for edge estimation even in the NVC case as can be seen in Figs. 7–9, where the topology of networks inferred by PLI-NVC is very close to random networks, see Fig. 13. It is well known that PC and coherence are affected by the amplitude of the sources and also volume conduction, being PC affected by this latter one only. Furthermore, as mentioned in Vinck et al. (2011), PLI, R and PC are also influenced by the length of the time series. In our experiments, all comparison tests were made with time series of same length, hence this parameter does not affect our final conclusion, the small-worldness shown by PLI networks.

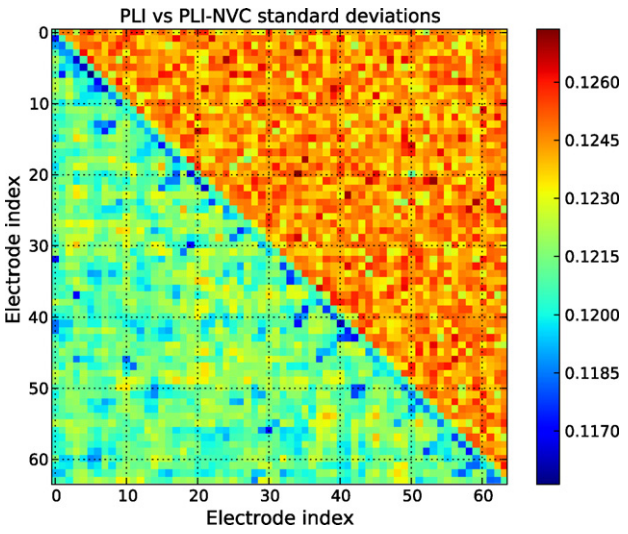

Fig. 14. PLI distributions for volume and no-volume conduction. The matrix shows the standard deviation of the PLI histograms for the $N(N-1)/2$ possible pairs of electrodes. The lower triangular matrix has all standard deviations for the volume conduction case. The upper triangular matrix represents all standard deviations of PLI histograms without volume conduction.

In this paper we tested PLI performance under the null hypothesis. However, a true delayed interaction will not be affected by the issues shown in this paper. The interaction among two sources with a true delay will cause an asymmetric phase distribution easily estimated by PLI with a high index value, see Fig. 2 middle column. This makes necessary in the future the designing of strategies to identify true connectivity, and minimize the spurious clustering produced by the volume conduction problem. For instance, if a fixed degree D threshold strategy is used as in this paper, attention should be paid to those high degree nodes whose edges are close to the threshold value. Also, solving the inverse problem to work in the source domain instead of the sensor domain might diminish the PLI small-world bias.

7. Conclusions

In our experiments we applied PLI for brain network inference in EEG using the four sphere head model to simulate the volume conduction problem. We also tested PC and coherence for the same task. The performance of coherence and PC is well known in the literature. Both measures are highly affected by volume conduction, and coherence in particular is also affected by the time series amplitude. PLI is a newer and robust measure that has shown remarkable results in recently published work. PLI has the characteristic of being partially invariant to volume conduction, and also offers estimations for delayed synchronization between two sources.

The networks found by applying PLI to independent sources in a volume conduction environment were different from random networks, showing that volume conduction affects PLI inference. This

was not the case for PLI-NVC networks whose behaviour was very close to random networks. The volume conduction influence on PLI produces small-worldness in the estimated networks, a result that produces a bias in network analysis.

The results presented in this paper do not try to disqualify any of the techniques applied in our experiments, but to show their performance and make the Neuroscience community aware of their behaviour. Future work must focus on designing strategies to minimize the effect of volume conduction on network estimation.

Acknowledgement

This work was supported by the National Council on Science and Technology (CONACYT), Mexico, http://www.conacyt.gob.mx.

References

Bassett DS, Bullmore ED. Small-world brain networks. Neuroscientist 2006;12(6):512–23.
De Vico Fallani F, Astolfi L, Cincotti F, Mattia D, la Rocca D, Maksuti E, et al. Evaluation of the brain network organization from EEG signals: a preliminary evidence in stroke patient. Anat Rec 2009;292:2023–31.
Granger CWJ. Investigating causal relations by econometric models and cross-spectral methods. Econometrica 1969;37(3):424–38.
Guevara R, Perez Velazquez JL, Nenadovic V, Wennberg R, Senjanovic G, Dominguez LG. Phase synchronization measurements using electroencephalographic recordings. What can we really say about neuronal synchrony? Neuroinformatics 2005;05:301–14.
Halliday DM, Conway BA, Farmer SF, Rosenberg JR. Using electroencephalography to study functional coupling between cortical and electromyograms during voluntary contractions in humans. Neurosci Lett 1998;241:5–8.
Halliday DM, Roserberg JR, Amjad AM, Breeze P, Conway BA, Farmer SF. A framework for the analysis of mixed time series/point process data—theory and applications to the study of physiological tremor, single motor unit discharges and electromyograms. Prog Biophys Mol Biol 1995;64(2/3):273–8.
Hayes MH. Statistical digital signal processing and modelling. John Wiley & Sons; 1996, 194.
He Y, Chen ZJ, Evans AC. Small-world anatomical networks in the human brain revealed by cortical thickness from MRI. Cereb Cortex 2007;17(10):2407–19.
Micheloyannis S, Vourkas M, Tsirka V, Karakonstantali E, Kanatsouli K, Stam CJ. The influence of ageing on complex brain networks: a graph theoretical analysis. Hum Brain Mapp 2009;30(1):200–8.
Milo R, Shen-Orr S, Itzkovitz S, Kashtan N, Chklovskii D, Alon U. Network motifs: simple building blocks of complex networks. Science 2002;298:824–7.
Mormann F, Lehnertz K, David P, Elger CE. Mean phase coherence as a measure for phase synchronization and its application to the EEG of epilepsy patients. Physica D 2000;144(3–4):358–69.
Newman MEJ. Networks an introduction. Oxf. Univ. Press; 2010, 185.
Nichols TE, Holmes AP. Nonparametric permutation tests for functional neuroimaging: a primer with examples. Hum Brain Mapp 2002;15(1):1–25.
Nolte G, Bai O, Wheaton L, Mari Z, Vorbach S, Hallet M. Identifying true brain interaction from EEG data using the imaginary part of coherency. Clin Neurophysiol 2004;115:2292–307.
Nunez PL, Silberstein RB, Shi Z, Carpenter MR, Srinivasan R, Tucker DM, et al. EEG coherency II: experimental comparisons of multiple measures. Clin Neurophysiol 1999;110:469–86.
Nunez PL, Srinivasan R, Westdorp AF, Wijesinghe RS, Tucker DM, Silberstein RB, et al. EEG coherency I: statistics, reference electrode, volume conduction, Laplacians, cortical imaging, and interpretation at multiple scales. Electroencephalogr Clin Neurol 1997;103:499–515.
Nunez PL, Srinivasan R. Electric fields of the brain—the neurophysics of EEG (2nd ed.). Oxf. Univ. Press; 2006, 256.
Quiroga RQ, Kraskov A, Kreuz T, Grassberger P. Performance of different synchronization measures in real data: a case study on electroencephalographic signals. Phys Rev E 2002;65(4):041903.
Rosenberg JR, Amjad AM, Breeze P, Brillinger DR, Halliday DM. The Fourier approach to the identification of functional coupling between neuronal spike trains. Prog Biophys Mol Biol 1989;53:1–31.
Rubinov M, Sporns O. Complex network measures of brain connectivity: uses and interpretations. Neuroimage 2009;52(3):1059–69.
Sameshima K, Baccalá LA. Using partial directed coherence to describe neuronal ensemble interactions. J Neurosci Methods 1999;94(1):93–103.
Scannell JW, Blakemore C, Young MP. Analysis of connectivity in the cat cerebral cortex. J Neurosci 1995;15:1463–83.
Schoffelen JM, Gross J. Source connectivity analysis with MEG and EEG. Hum Brain Mapp 2009;30:1857–65.
Sporns O, Zwi JD. The small world of the cerebral cortex. Neuroinformatics 2004;2:145–62.
Sporns O, Honey CJ. Small worlds inside big brains. Proc Nat Acad Sci USA 2006;103(51):19219–20.
Stam CJ, Dijk BWV. Synchronization likelihood: an unbiased measure of generalized synchronization in multivariate data sets. Physica D 2002;163:236–51.
Stam CJ, Nolte G, Daffertshofer A. Phase lag index: assessment of functional connectivity from multi channel EEG and MEG with diminished bias from common sources. Hum Brain Mapp 2007;28(11):1178–93.
Tass P, Rosenblum MG, Weule J, Kurths J, Pikovsky A, Volkmann J, et al. Detection of n:m phase locking from noisy data: application to magnetoencephalography. Phys Rev Lett 1998;81:3291–4.
Vinck M, Oostenveld R, van Wingerden M, Battaglia F, Pennartz CMA. An improved index of phase-synchronization for electrophysiological data in the presence of volume-conduction, noise and sample-size bias. Neuroimage 2011;55:1548–65.
Watts DJ, Strogatz SH. Collective dynamics of "small world" networks. Nature 1998;393:440–2.
Wheaton LA, Nolte G, Bohlhalter S, Fridman E, Hallet M. Synchronization of parietal and premotor areas during preparation and execution of praxis hand movements. Clin Neurophysiol 2005;116:1382–90.
Young MP. Objective analysis of the topological organization of the primate cortical visual system. Nature 1992;358:152–5.
Zhang Z, Zhang J. A big world inside small-world networks. Plos One 2009;4(5).